Square, Hexagonal, and Row Phases of PTCDA and PTCDI on Ag−Si(111)$\sqrt{3} \times \sqrt{3}R30°$

J. C. Swarbrick,[†] J. Ma,[†] J. A. Theobald,[†] N. S. Oxtoby,[‡] J. N. O'Shea,[†] N. R. Champness,[‡] and P. H. Beton*,[†]

School of Physics and Astronomy, University of Nottingham, University Park, Nottingham NG7 2RD, U.K., and School of Chemistry, University of Nottingham, University Park, Nottingham NG7 2RD, U.K.

Received: February 17, 2005; In Final Form: April 27, 2005

We have investigated the ordered phases of the perylene derivatives perylene-3,4,9,10-tetracarboxylic-3,4,9,-10-dianhydride (PTCDA) and the imide analogue PTCDI on the Ag−Si(111)$\sqrt{3} \times \sqrt{3}R30°$ surface using scanning tunneling microscopy. We find that PTCDA forms square, hexagonal, and herringbone phases, which coexist on the surface. The existence of a square phase on a hexagonal surface is of particular interest and is a result of a near commensurability between the molecular dimensions and the surface lattice. Contrast variations across the square islands arise from PTCDA molecules binding to different sites on the surface. PTCDI on Ag−Si(111)$\sqrt{3} \times \sqrt{3}R30°$ forms extended rows, as well as two-dimensional islands, both of which are stabilized by hydrogen bonding mediated by the presence of imide groups. We present models for the molecular arrangements in all these phases and highlight the role of hydrogen bonding in controlling this order.

1. Introduction

The investigation into the effects of hydrogen bonding on two-dimensional arrangements of adsorbed molecular systems is currently of great interest.[1] Hydrogen bonding has been shown to stabilize a wide range of ordered molecular arrays, from clusters and rows[2−4] to more complicated open structures.[5−7] Much of this work has focused on metal substrates under ultrahigh vacuum and low temperature conditions,[8,9] but more recently, hydrogen bond mediated ordering has also been demonstrated for semiconductor substrates, and molecular frameworks have been demonstrated as templates for nanostructure formation.[10]

In this paper, we study the role of hydrogen bonding in the stabilization of surface phases of the perylene derivatives perylene-3,4,9,10-tetracarboxylic-3,4,9,10-dianhydride (PTCDA) and the imide analogue PTCDI on Ag−Si(111)$\sqrt{3} \times \sqrt{3}R30°$. The closely related, but smaller, molecules naphthalene-3,4,9,-10-tetracarboxylic- 3,4,9,10-dianhydride (NTCDA) and imide (NTCDI), which have a smaller naphthalene core but the same functional end groups, have previously been studied by Keeling et al. on Ag−Si(111)$\sqrt{3} \times \sqrt{3}R30°$.[11] The work presented below represents an important extension of these previous studies, since the study of the larger molecules PTCDA and PTCDI is expected to provide insight into the relative importance of surface commensurability and hydrogen bonding in molecular ordering.

In addition, the study of PTCDA and PTCDI as molecular adsorbates is important in its own right. PTCDA has been widely studied as a candidate material for organic electronic devices[12] and is also known to form many different ordered surface phases. The ordering of PTCDA monolayers and thin films has been studied on noble metal surfaces,[13,14] highly ordered pyrolytic graphite (HOPG),[15] passivated noble metal surfaces,[16] semiconductor surfaces,[17,18] and self-assembled organic monolayers.[19,20] PTCDI is also of potential importance for organic semiconductor devices,[21] and its adsorption on several surfaces has been investigated previously.[22]

In fact, the behavior of PTCDA and PTCDI shows important differences but also some similarities to previous observations of NTCDA and NTCDI. In addition, both PTCDA and PTCDI, when adsorbed on the Ag−Si(111)$\sqrt{3} \times \sqrt{3}R30°$ surface, show pronounced differences compared with the ordering observed on other substrates. As we show below, PTCDA forms three different coexisting phases. A herringbone phase is observed, with rows running along the three principal directions on the Ag−Si(111)$\sqrt{3} \times \sqrt{3}R30°$ reconstruction. This herringbone phase shows contrast variations between neighboring rows which we attribute to adsorption on different surface binding sites. Second, a close-packed square phase is observed, which is unexpected for a hexagonal substrate but has previously been proposed for a PTCDA layer on Au(111).[20] The final phase is a hexagonal network, which has two chiral forms and may be understood as a combination of the herringbone and square phases. PTCDI shows a completely different behavior, arranging into extended single rows along the principal surface reconstruction directions. These rows coexist with two-dimensional quasi-hexagonal close-packed islands.

2. Experimental Details

Images were acquired at room temperature using a scanning tunneling microscope (STM) operating in constant current mode in an ultrahigh vacuum (UHV) system (base pressure 1×10^{-10} Torr). Electrochemically etched tungsten tips were used, which were cleaned prior to use by electron beam heating. Atomically clean Si(111) was prepared by degassing a piece of p-type Si-(111) wafer and then heating by direct current to 1150 °C. The quality of the resulting (7×7) reconstruction was checked using a STM, and silver was then deposited while the sample was heated to 550 °C, to form the Ag−Si(111)$\sqrt{3} \times \sqrt{3}R30°$ reconstruction.[23] The adsorption of several organic molecules has previously been studied on this surface.[11,24]

* Corresponding author. E-mail: peter.beton@nottingham.ac.uk.
[†] School of Physics and Astronomy.
[‡] School of Chemistry.

10.1021/jp0508305 CCC: $30.25
Published on Web 05/26/2005

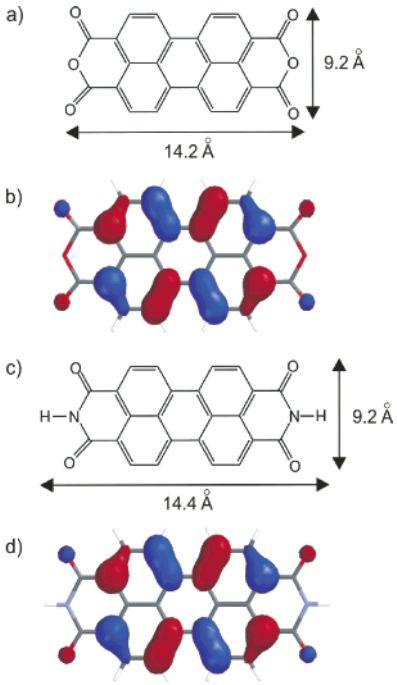

Figure 1. (a and b) PTCDA and (c and d) PTCDI molecules. The molecular dimensions are shown in images a and c. Each molecule has a perylene core, but PTCDA has anhydride groups at the ends, while PTCDI has imide groups. The molecular structures of (b) PTCDA and (d) PTCDI are calculated using the semiempirical AM1 model. This figure shows the spatial variation of the probability amplitude of the highest occupied molecular orbitals (HOMOs). Red and blue represent respectively regions of positive and negative probability amplitude.

The structures of PTCDA and PTCDI are shown in Figure 1. PTCDA (Sigma-Aldrich, 99.9% pure) was thoroughly degassed prior to deposition at 330 °C for 10 min, to give a submonolayer coverage (~0.1 ML). PTCDI was prepared by refluxing PTCDA in concentrated ammonia for ~15 h[25] and, following purification and degassing, was deposited by heating to 335 °C for up to 10 min for a submonolayer coverage (up to 0.4 ML). The substrate was held at room temperature when depositing both PTCDA and PTCDI. The preparation and imaging of all samples was undertaken in the same UHV system.

The molecular structure and dimensions of the observed phases were calculated using Spartan'02 software, using semiempirical molecular orbit calculations within the AM1 model. The spatial distribution of the HOMOs of PTCDA and PTCDI were calculated for isolated molecules and are shown in Figure 1. There is a clear minimum in the HOMO of each molecule along the long axis. On the basis of these simple models, one may expect both molecules to have a similar appearance in filled state STM images. Semiempirical modeling was also used as a simple check to test the validity of proposed models for the different observed molecular phases. The surface was not included in the calculations. Small clusters of molecules were arranged as in the proposed model arrangements for the phases observed, and the clusters were minimized in the AM1 model to determine whether the phases were stable and to obtain estimates for intermolecular spacings.

3. Phases of PTCDA

STM images of the surface after the deposition of ~0.1 ML of PTCDA are shown in Figure 2. Islands of PTCDA are formed with lateral dimensions up to 300 nm, often growing from step edges (Figure 2a) or between steps on the Ag−Si(111)$\sqrt{3} \times \sqrt{3}R30°$ surface. Three distinct phases were observed, which will be referred to as the square phase, the herringbone phase, and the hexagonal phase. All three phases have been observed to coexist in a single island, as in Figure 2b. The islands have a topographic height of 2.4 ± 0.5 Å, consistent with a single layer of molecules lying flat on the surface, as expected for a large π-conjugated molecule.

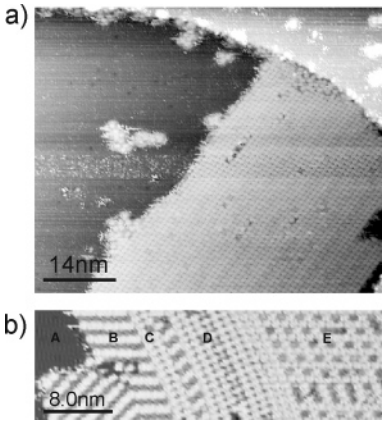

Figure 2. (a) An island of PTCDA stabilized by growing from a step edge. This island consists only of the square phase. (b) A section of a multiphase island of PTCDA: A, silver termination; B, herringbone phase; C, boundary row; D, square-packed phase; E, hexagonal phase. For both images, bias = −3.0 V and current = 0.1 Na.

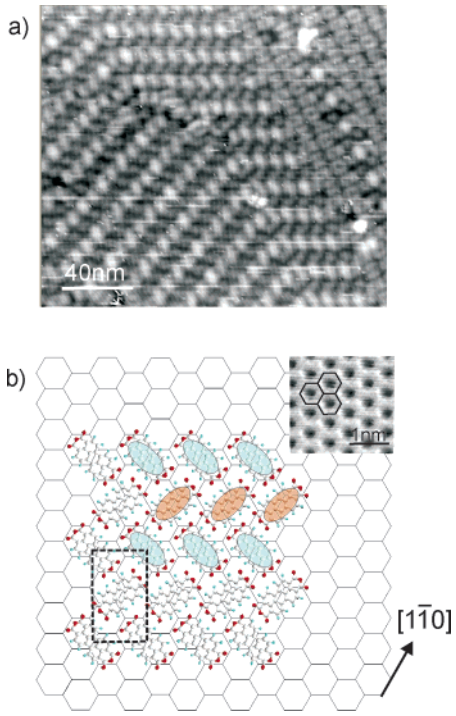

Figure 3. (a) Two domains of the herringbone phase are shown. The square phase appears in the top left of the image (section 3.2) (bias = 2.0 V, current = 0.1 nA). (b) This model shows the molecules sitting in inequivalent sites in alternate horizontal rows on the Ag−Si(111) $\sqrt{3} \times \sqrt{3}R30°$ surface, which would account for the contrast variation seen in the images. [1$\bar{1}$0] is the underlying Si lattice vector. The inset in part b shows an STM image of the Ag−Si(111)$\sqrt{3} \times \sqrt{3}R30°$ reconstruction (see text) (bias = 2.0 V, current = 0.1 nA).

3.1. Herringbone Phase. Figure 3a shows an STM image in which one of the principal phases is clearly resolved. The phase is composed of alternating rows of canted molecules, which run along the major axes of the Ag−Si(111)$\sqrt{3} \times$

$\sqrt{3}R30°$ termination. Each molecule appears as a single bright topographic feature with an apparent height which alternates from row to row.

The silver termination is shown in the inset of Figure 3b and may be represented by a hexagonal network. According to the widely accepted model for the atomic configuration of the surface (the honeycomb chain trimer model[23]), the network vertices correspond to silver trimers and a silicon trimer is positioned at the center of each hexagonal repeat unit. All dangling bonds are saturated on this surface, rendering it relatively passive so that molecules are free to diffuse across the surface and adopt ordered configurations which are determined by intermolecular interactions. The underlying silicon lattice vector $[1\bar{1}0]$ is indicated on all models as a reference direction.

The separation between equivalent rows is determined from images in which the silver termination and the molecular overlayer are both resolved and found to be $3a$ (where a = 6.65 Å is the lattice constant of the Ag−Si(111)$\sqrt{3} \times \sqrt{3}R30°$ surface). From similar images, the molecular separation within a row has been determined by measurement from images as $\sqrt{3}a$. This forms the basis for the model shown in Figure 3b; here, the unit cell of the molecular packing is shown as $3a \times \sqrt{3}a$, or 20.01 Å × 11.55 Å. A similar herringbone phase has been reported on many other surfaces.[14−16,20] The bulk α phase of PTCDA is monoclinic and is composed of stacked planes of molecules in a herringbone packing. The unit cell dimensions are 19.91 Å × 11.96 Å for the bulk herringbone unit cell.[14] These values are close to the unit cell dimensions observed in this work and others,[26] and within experimental error, the molecular angles are the same for this phase and in the bulk α phase. Semiempirical modeling using the AM1 model of a planar cluster of six PTCDA molecules gives optimum unit cell dimensions of 19.5 Å × 12.1 Å, in reasonable agreement with observed dimensions.

The difference in contrast of adjacent rows indicates that molecules are sitting at inequivalent binding sites on the surface. In Figure 3b, a possible registry with the surface in which alternate rows are adsorbed on inequivalent sites, which is consistent with the observed contrast variation, is shown. Similar contrast variations have previously been reported in herringbone phases of PTCDA on different substrates.[15,27]

3.2. Square Phase. The second principal phase is shown in Figures 2a and 4. The apparent square arrangement of these molecules is very unusual; the molecules are adsorbed on a hexagonal substrate, which would not be expected to support an overlayer with square symmetry. Also, in images such as Figure 4a, it is possible to resolve intramolecular contrast in the form of two lobes running along the length of each molecule. We associate these lobes with the HOMO calculated using a semiempirical model (see Figure 1), and our images show that nearest neighbors are perpendicular to each other and form an arrangement which is very close to a candidate structure proposed by Staub et al.[20] It is clear that this phase is stable, as extended, well ordered regions are observed (Figure 2a).

Images where both the hexagonal Ag−Si(111)$\sqrt{3} \times \sqrt{3}R30°$ surface reconstruction and square-packed molecular islands are well resolved, such as that in Figure 4c, show that one axis of the square phase is parallel to the $[1\bar{1}0]$ direction of the underlying silicon surface. Also, the separation of the centers of two equivalent molecules in this direction may be accurately measured as $2\sqrt{3}a$, or 23.1 Å, from the construction in Figure 4c. Note that alternate molecules in rows running in the $[1\bar{1}0]$ direction are in equivalent surface adsorption sites; see the models in Figure 5.

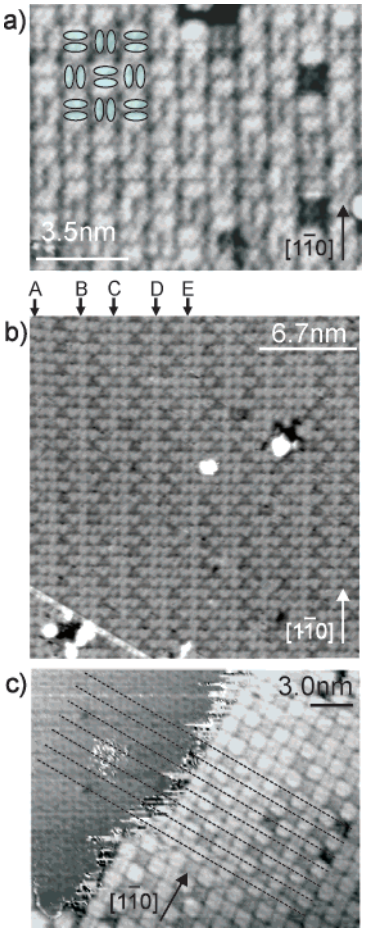

Figure 4. STM images of the square phase: (a) In this image, intermolecular contrast is resolved, showing that adjacent molecules are perpendicular to each other. This is illustrated by the schematic overlay of the lobes of the HOMO over the intramolecular features (bias = −3.0 V, current = 0.1 nA). (b) A larger square-packed region showing contrast variation between different molecules; the letters A−E are explained in the text (bias = −2.5 V, current = 0.1 nA). (c) This image shows the initial steps in determining the registry of PTCDA molecules in the square phase. The silver termination is resolved in the upper left part of the image, and the dotted lines show the separation of molecules with respect to the silver termination (bias = −2.5 V, current = 0.1 nA).

It is much more difficult to identify the separation of the adsorption sites in the rows running perpendicular to the $[1\bar{1}0]$ direction. Within experimental error, the molecular spacing in the two orthogonal directions is equal. We have considered possible models for commensurate arrangements in which n molecular repeat units (consisting of two orthogonal molecules) are placed over m lattice constants. For n repeat units, the unit cell dimension in the $[1\bar{1}0]$ direction is $2n\sqrt{3}a$. From a simple consideration of the geometry of square and hexagonal lattices, it is clear that we must identify a pair of integers n and m which satisfy the relationship $2n\sqrt{3}a = ma$, that is, give a molecular repeat unit with sides of equal length. Although this equality cannot be satisfied exactly, since $\sqrt{3}$ is an irrational number, there are two pairs of integers (n,m) for which this condition holds to within 1%. These integer pairs are (2,7) and (7,24), and the resulting values for the molecular separation are shown in Table 1. Note that the molecular repeat unit length is given by ma/n, which is equal to 23.3 and 22.8 Å, respectively, for the (2,7) and (7,24) models. These values correspond to a 1%

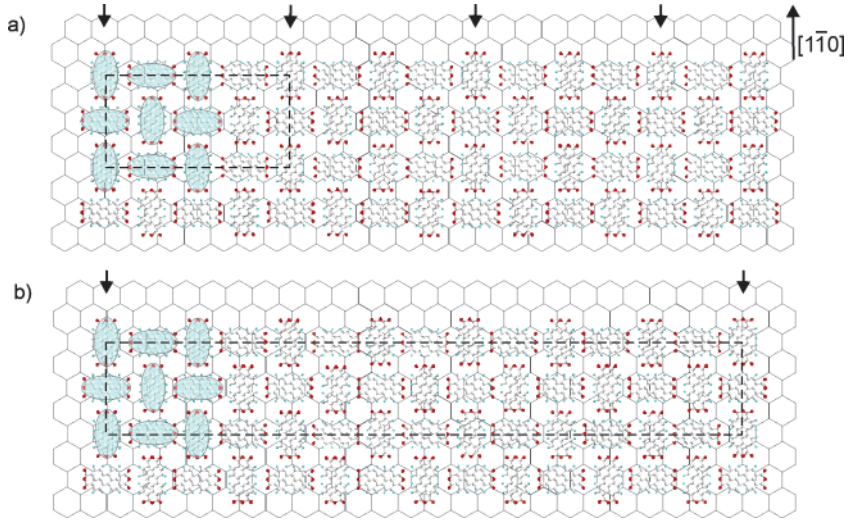

Figure 5. The two molecular models considered for this phase. Part a has unit cell dimensions of $2\sqrt{3}a \times 7a$, and part b shows an alternative model with a larger unit cell of $2\sqrt{3}a \times 24a$. The unit cells are shown with dotted lines. The small arrows highlight molecules in equivalent binding sites if looking perpendicular to the [1$\bar{1}$0] direction (indicated). This helps to show the 2- and 7-fold periodicity of molecular pairs.

TABLE 1: Summary of Two Possible Square Phase Dimensions[a]

n,*m*	$2n\sqrt{3}$	*ma*/*n* (Å)	$1 - (m/2n\sqrt{3})$ (%)
$n = 2, m = 7$	6.93	23.3	−1.0
$n = 7, m = 24$	24.25	22.8	+1.0

[a] This table summarizes the dimensions of two possible commensurate arrangements of molecules in rows perpendicular to the [1$\bar{1}$0] direction of the Si substrate. The commensurability corresponds to *n* orthogonal molecular pairs over *m* lattice constants. The integers *n* and *m* are given in column 1. Column 2 gives the dimension of the unit cell along the [1$\bar{1}$0] direction in units of the surface lattice constant; this value should be close to *m*. Column 3 gives the average length in the direction perpendicular to [1$\bar{1}$0] occupied by an orthogonal molecular pair, and column 4 gives the percent difference between the molecular spacing parallel and perpendicular to the [1$\bar{1}$0] direction; a positive value indicates that rows perpendicular to [1$\bar{1}$0] are compressed.

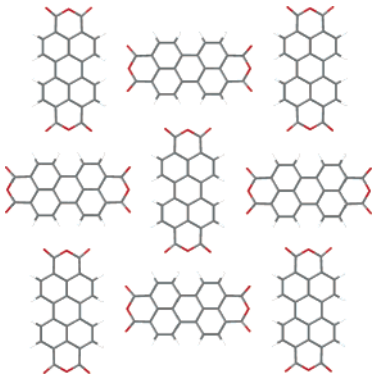

Figure 6. The semiempirical model of a nine-molecule cluster in the square phase as calculated by Spartan gives a distance between equivalent molecules of 22.8 Å.

extension and compression compared with the spacing in the [1$\bar{1}$0] direction.

The stability of the proposed arrangements has been investigated using semiempirical modeling as described above. The AM1 model has been used to minimize the total energy of the planar cluster of nine PTCDA molecules shown in Figure 6 (and also smaller clusters down to two molecules only). Our simulations confirm that this arrangement is stable with a calculated separation between equivalent molecules of 22.8 Å. The perpendicular orientation of neighboring molecules is stabilized by weak C−H···O hydrogen bonding between the dianhydride groups and the hydrogen atoms bonded to the perylene core of PTCDA, as discussed by Chen et al.,[26] in combination with the quadrupolar interaction between PTCDA molecules.[20] The calculated spacing, 22.8 Å, is very close to the molecular repeat unit in the proposed models both parallel and perpendicular to the [1$\bar{1}$0] direction.

It is possible to distinguish experimentally between the (2,7) and (7,24) models for molecular packing by acquiring images with the sample bias in the range from −2.0 to −2.5 V. Over this bias range, we observe a contrast variation between molecules adsorbed at different surface sites.

Figure 4b shows a STM image of a region of the square-packed phase acquired in this bias range. The resulting contrast variation has the appearance of stripes running in the [1$\bar{1}$0] direction, since molecules in the rows running in this direction are adsorbed in equivalent sites (although note that neighboring molecules are orthogonal, resulting in a contrast difference between alternate molecules, giving some of the rows in this direction a 2-fold periodicity).

There is a more complex contrast variation perpendicular to the [1$\bar{1}$0] direction which arises from the occupancy of many nonequivalent surface sites in the rows running in this direction. However, a variation in apparent brightness is observed only for one of the two possible orthogonal molecular orientations. Specifically, molecules oriented with their long axis perpendicular to the [1$\bar{1}$0] direction show strong variations in molecular contrast for different adsorption sites along the rows running perpendicular to the [1$\bar{1}$0] direction. However, for molecules with their long axis along the [1$\bar{1}$0] direction, the variation in contrast is much weaker. The formation of one of the commensurate structures discussed above would give rise to a regular sequence of stripes (parallel to [1$\bar{1}$0]) with a period (in the direction perpendicular to [1$\bar{1}$0]) corresponding to *n* molecular repeat units. For the (2,7) proposed array, the contrast would be periodic with a period corresponding to *n* pairs of orthogonal molecules; that is, every fourth row running along the [1$\bar{1}$0] axis would be equivalent. Similarly, for the (7,24) array, every 14th row would be equivalent.

In most of our images, it is difficult to pick out a clear repeating sequence. We see some evidence for the (7,24) ordering, as shown in Figure 4b. As marked on this figure (A−E), we see double and single bright rows running along [1$\bar{1}$0] which are alternately separated by three or four molecules (e.g.,

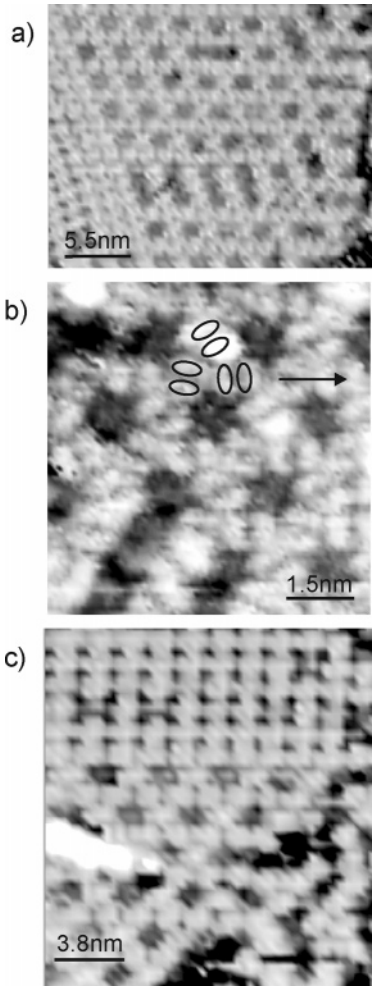

Figure 7. (a) Extended region of the hexagonal open phase (bias = −3.0 V, current = 0.1 nA). (b) The resolved lobes of the molecules (see Figure 4a), indicating their orientations. These are highlighted, and the [1$\bar{1}$0] direction is indicated (bias = −3.0 V, current = 0.1 nA). (c) The hexagonal phase neighboring a square phase region (bias = −3.0 V, current = 0.1 nA).

the separation of A and B is four molecules, the separation of B and C is three molecules, etc.). This ordering is consistent with an overall periodicity of seven molecular repeat units, although, unsurprisingly for such a large unit cell, we do not observe this sequence repeating over multiple unit cells. Although we observe some local order with a repeat unit of four molecules, we see no evidence for extended regions showing the (2,7) ordering, which, for this smaller unit cell, would be expected if it were the preferred configuration. Overall, we conclude from our experimental data that the (7,24) ordering is more stable, while noting that the combination of a large unit cell, many possible (7) nonequivalent adsorption sites and the presence of defects on the surface limits the formation of domains displaying this order over many unit cells. Indeed, even for surfaces with relatively low defect densities as prepared for these studies, it is difficult to distinguish experimentally the formation of commensurate packing with such a large unit cell from an incommensurate arrangement.

3.3. Hexagonal Phase. STM images of the third major phase of PTCDA, the hexagonal phase, are shown in Figure 7. Figure 7a shows an extended region of this phase, while Figure 7b shows a higher magnification image in which intramolecular features may be resolved. These features, two lobes, are very similar to those observed for molecules in the square phase (see section 3.2). The hexagonal phase was seen in two chiral arrangements. Analysis of profiles across the phase shows that the darkest features are not empty pores, since they do not have the same apparent height as the silver termination. These features correspond to molecules which have a low apparent brightness, similar to the dark rows in the herringbone phase (section 3.1). The separation between low contrast molecules is equal to 2$\sqrt{3}a$.

Hexagonal and square phases coexist in the same island with no disordered boundary where they meet, as seen in Figure 7c. The horizontal rows of the square phase are parallel to rows in the hexagonal phase, and in fact, the bright rows of the hexagonal phase have a nearly equivalent appearance to the rows of the square phase. Hexagonal and herringbone phases also coexist in the same island with no disordered boundary between them, as shown in Figure 7a. In this case, the horizontal rows in the hexagonal phase which appear alternately bright and dark are parallel and very similar to rows of the herringbone phase (with alternate bright and dark contrast molecules) which run along the [1$\bar{1}$0] direction.

By examining images of multiphase islands, it is possible to determine, to a first approximation, that this phase is composed of alternating rows of molecules in the square and herringbone configurations. The model for this arrangement is shown in Figure 8. We have analyzed the proposed molecular arrangement using numerical modeling. The AM1 semiempirical model was used to minimize the energy of the cluster shown in Figure 9, and our results confirm that this arrangement of molecules is stable. However, the molecular configurations relax slightly from those shown in Figure 8a which correspond exactly to alternate rows of square and hexagonal phases. The relaxed configuration is shown in Figure 8b. Note that within the square phase rows the molecules are rotated through ∼5° to relax the molecular arrangement and allow optimum hydrogen bonding geometries. This is consistent with the observed orientation of the molecules (see highlighted intramolecular structure in Figure 7b).

The packing fractions of the three observed phases along with the packing fraction of molecules in the bulk α phase are in Table 2 as a summary. The herringbone phase has the highest packing, while the symmetrical square and hexagonal surface phases have a lower density than the bulk α phase. This implies the new 2-D phases we have observed are stabilized by interactions with the substrate.

4. Phases of PTCDI

4.1. 1-D Rows. PTCDI differs from PTCDA through the replacement of the central oxygen atom of each anhydride group with an N−H imide group. This results in a modification of the hydrogen bonding between neighboring molecules. For PTCDA, a rectangular molecule, the anhydride groups promote hydrogen bonding between the short (anhydride group) and long (the perylene core) molecular edges, resulting in the perpendicular, or near-perpendicular, arrangement of neighboring molecules. Incorporation of the imide group is expected, through the presence of the hydrogen atom of the imide group, to inhibit the hydrogen bonding observed for PTCDA and simultaneously promote much stronger N−H···O hydrogen bonding between the imide groups on neighboring molecules. Overall, this is expected to result in the formation of rows stabilized by hydrogen bonding between the ends of molecules as previously observed for NTCDI.

For very low coverages (<0.02 ML) of PTCDI on Ag−Si(111)$\sqrt{3} \times \sqrt{3}R30°$, we observe molecules which either are isolated or form rows with a width equal to a single molecule. These rows are aligned with the principal axes of the Ag−Si-

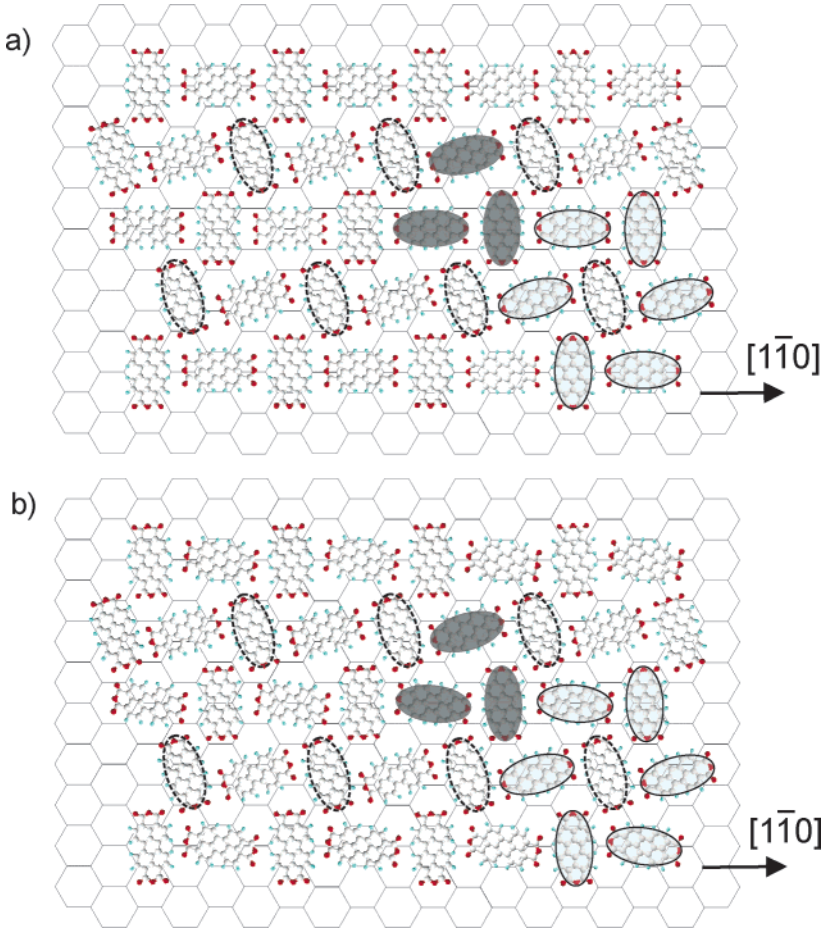

Figure 8. (a) This inital model shows the combination of square and herringbone phase rows which comprise the hexagonal phase. (b) This model shows the relaxed form, with the molecules oriented to give a valid hydrogen bonding configuration. A triangular unit equivalent to that in Figure 7b is shown by dark ovals, and a hexagonal unit is highlighted by pale outlined ovals. The molecules of low contrast in the images are shown with dotted oval outlines. This model is valid for the chiral version observed for this phase.

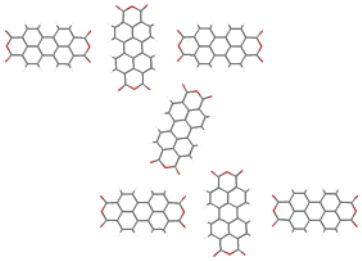

Figure 9. The semiempirical model of a seven-molecule cluster in the hexagonal phase, made of two three-molecule square phase rows and a central herringbone molecule as calculated by Spartan. The angle of the long axis of the central molecule from the vertical is 22°.

TABLE 2: Packing Fractions of PTCDA Phases[a]

phase	packing fraction (Å^2 per molecule)
herringbone	114.9
bulk α phase	119.1
square (2,7)	134.1
square (7,24)	131.3
hexagonal	134.1

[a] This table gives the packing fractions of the observed phases of PTCDA in terms of area per molecule as well as the packing fraction for the bulk α phase to compare with the herringbone phase. Note the packing fractions for the two proposed models for the square phase are given. The herringbone phase is the most close-packed phase.

$(111)\sqrt{3} \times \sqrt{3}R30°$ reconstruction, as shown in Figure 10a. This behavior is similar to that seen for NTCDI on the same surface[11] and also for PTCDI on hydrogen terminated silicon.[22]

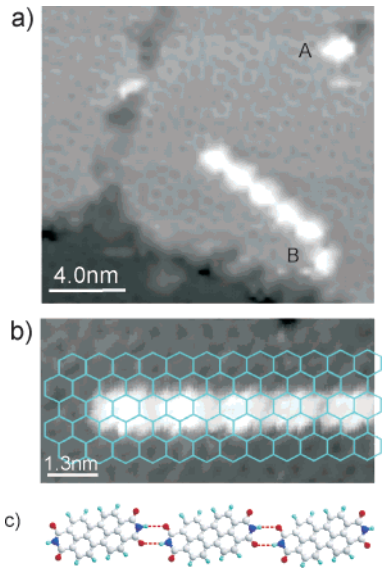

Figure 10. PTCDI forms one-dimensional rows: (a) single molecules adsorb at A, and rows extend from B, defects in the surface (bias voltage = −2.0 V); (b) the rows have a molecular separation of 14.1 ± 0.2 Å (bias voltage = −2.0 V); (c) the proposed model shows the rows to be stabilized by hydrogen bonds between imide groups.

Isolated molecules are adsorbed on defects on the surface. Many rows grow from defects and step edges, implying that these sites act as nucleation centers. In high resolution images such as Figure 10b, the silver termination and the PTCDI rows may

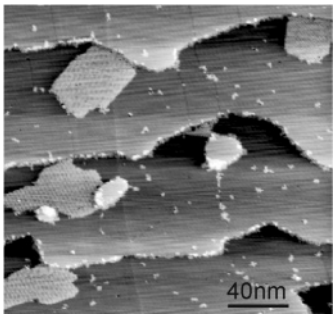

Figure 11. PTCDI forms two-dimensional islands at coverages of >0.02 ML which grow from steps on the Ag−Si(111)$\sqrt{3} \times \sqrt{3}R30°$ surface. The bias voltage is −2.0 V.

be resolved. The molecular separation is measured to be 14.1 ± 0.2 Å, and the molecules are canted by 8 ± 2° within the rows, to promote hydrogen bonding between imide groups. Typical rows have a length of approximately five molecules, with the longest observed being nine molecules. In the bulk crystalline form, PTCDI molecules are arranged in rows with an intermolecular spacing of 14.4 ± 0.2 Å and are canted through an angle of 9.2°, very close to that measured for rows of adsorbed molecules, as shown in Figure 10c. Very similar rows were observed when the smaller molecule NTCDI was deposited on the Ag−Si(111)$\sqrt{3} \times \sqrt{3}R30°$ surface. However, for NTCDI, the intermolecular spacing is commensurate with the lattice constant of the underlying surface and the stability of the rows, which extend over up to 25 NTCDI molecules, was attributed to this commensurability. For PTCDI, a commensurate intermolecular spacing is not observed (note that we cannot rule out a commensurate arrangement with a molecular repeat unit of greater than six molecules). In addition, the PTCDI rows are not kinetically stable, and molecules are transferred to two-dimensional islands (see below) on a time scale of a few days. The reduced stability of PTCDI rows, as compared with NTCDI, is attributed to the lack of commensurability for PTCDI.

4.2. 2-D Islands. As the coverage increases (>0.02 ML), two-dimensional islands form; see Figure 11. At this coverage, some short rows still exist but the majority of PTCDI molecules are incorporated into islands. These islands, like the PTCDA islands, tend to grow from step edges and between steps. However, the molecular arrangements of PTCDI and PTCDA differ significantly. A close-up of one of the PTCDI islands is shown in Figure 12a. The perpendicular arrangement of neighboring molecules observed for PTCDA is not seen, and the islands consist of arrays of rows of collinear molecules.

As for the PTCDI rows, this arrangement is stabilized by hydrogen bonding between the ends of adjacent molecules. However, unlike the PTCDI rows with a width of a single molecule, the rows within the 2-D islands are not aligned with the principal axes of the Ag−Si(111)$\sqrt{3} \times \sqrt{3}R30°$ surface. A higher magnification image of one island is shown in Figure 11a. From images such as these, the intermolecular spacing and orientation of the rows (relative to Si[11$\bar{2}$]) are measured to be 14.6 ± 0.2 Å and 12.2 ± 0.3°, respectively. A model which is consistent with the observed molecular arrangement is shown in Figure 12b. The intermolecular separation and row orientation given by this model are 14.75 Å and ±12°, respectively.

5. Discussion

In this STM study, we have compared the phases which result from the incorporation of an imide group into the molecule

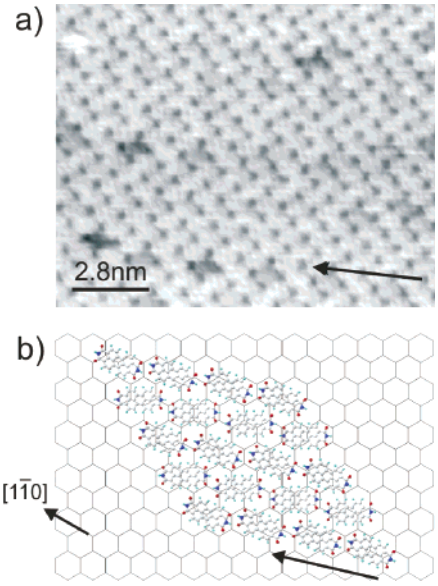

Figure 12. (a) This image shows the internal structure of the islands. The arrow shows the direction of the rows making up the island. The bias voltage is −2.0 V. (b) The molecular model for PTCDI islands. The rows are oriented at ±12° to Si[11$\bar{2}$]. As before, the row direction is indicated by the longer arrow, and the [1$\bar{1}$0] direction is shown.

PTCDA to form PTCDI. The sizes of these two molecules are almost equal, but the introduction of the imide group disrupts the hydrogen bonding which promotes a near-perpendicular arrangement of neighboring PTCDA molecules. The preferred perpendicular arrangement of PTCDA molecules results in the stabilization of the well-known herringbone phase and also gives rise, for the surface studied here, to a new square phase. The formation of the square phase is due to a commensurability between molecular dimensions and the surface lattice constant, although in one direction the resulting coincidence lattice extends over many molecular repeat units. The formation of a square phase on a hexagonal surface is an important observation and may give rise to the formation of new heteroepitaxial interfaces between materials with quite different crystal symmetries.

The incorporation of the imide group stabilizes the collinear arrangement of PTCDI molecules into rows which may be either isolated or form a regular array. This behavior is consistent with that observed previously for NTCDI, but there are some important differences. In particular, the absence of some simple commensurate arrangement of molecules within the single rows indicates that commensurability is not a universal requirement for the formation of molecular structures stabilized by noncovalent interactions. In many previous examples,[4,7,9−11] a regular array of molecules placed at surface sites are observed and the condition of commensurability might previously have been inferred to be a requirement in considering new candidate molecules for study.

Acknowledgment. We would like to thank Dr. M. Humphry for his assistance in this project, and we also acknowledge EPSRC for funding this work through the project GR/597521/01.

References and Notes

(1) De Feyter, S.; De Schryver, F. C. *Chem. Soc. Rev.* **2003**, *32*, 139−150.

(2) Bohringer, M.; Morgenstern, K.; Schneider, W.-D.; Berndt, R.; Mauri, F.; De Vita, A.; Car, R. *Phys. Rev. Lett.* **1999**, *83*, 324−327.

(3) Bohringer, M.; Schneider, M.; Berndt, R. *Surf. Rev. Lett.* **2000**, *7*, 661−666.
(4) Barth, J. V.; Weckesser, J.; Trimarchi, G.; Vladimirova, M.; De Vita, A.; Cai, C.; Brune, H.; Günter, P.; Kern, K. *J. Am. Chem. Soc.* **2002**, *124*, 7991−8000.
(5) Tanaka, H.; Nakagawa, T.; Kawai, T. *Surf. Sci. Lett.* **1996**, *364*, L575−L579.
(6) Furukawa, M.; Tanaka, H.; Kawai, T. *Surf. Sci.* **2000**, *445*, 1−10.
(7) Griessl, S.; Lackinger, M.; Edelwirth, M.; Hietschold, M.; Heckl, W. *Single Mol.* **2002**, *3*, 25−31.
(8) Nakagawa, T.; Tanaka, H.; Kawai, T. *Surf. Sci.* **1997**, *370*, L144−L148.
(9) Barth, J. V.; Weckesser, J.; Cai, C.; Günter, P.; Bürgi, L.; Jeandupeux, O.; Kern, K. *Angew. Chem., Int. Ed.* **2000**, *39*, 1230−1234.
(10) Theobald, J. A.; Oxtoby, N. S.; Phillips, M. A.; Champness, N. R.; Beton, P. H. *Nature* **2003**, *424*, 1029−1031.
(11) Keeling, D. L.; Oxtoby, N. S.; Wilson, C.; Humphry, M. J.; Champness, N. R.; Beton, P. H. *Nano Lett.* **2003**, *3*, 9−12.
(12) Hirose, Y.; Kahn, A.; Aristov, V.; Soukiassian, P.; Bulovic, V.; Forrest, S. R. *Phys. Rev. B* **1996**, *54*, 13748−13758.
(13) Wagner, T.; Bannani, A.; Bobisch, C.; Karacuban, H.; Stohr, M.; Gabriel, M.; Moller, R. *Org. Electron.* **2004**, *5*, 35−43.
(14) Glöckler, K.; Seidel, C.; Soukopp, A.; Sokolowski, M.; Umbach, E.; Bohringer, M.; Berndt, R.; Schneider, W.-D. *Surf. Sci.* **1998**, *405*, 1−20.
(15) Kendrick, C.; Kahn, A.; Forrest, S. R. *Appl. Surf. Sci.* **1996**, *104*/*105*, 586−594.
(16) Tiba, M.; Kurnosikov, O.; Flipse, C.; Koopmans, B.; Swagten, H.; Kohlhepp, J.; de Jonge, W. *Surf. Sci.* **2002**, *498*, 161−167.
(17) Nicoara, N.; Custance, O.; Granados, D.; García, J. M.; Gómez-Rodríguez, J. M.; Baró, A. M.; Méndez, J. *J. Phys.: Condens. Matter* **2003**, *15*, S2619−S2629.
(18) Sazaki, G.; Fujino, T.; Sadowski, J. T.; Usami, N.; Ujihara, T.; Fujiwara, K.; Takahashi, Y.; Matsubara, E.; Sakurai, T.; Nakajima, K. *J. Cryst. Growth* **2004**, *262*, 196−201.
(19) Schmitz-Hübsch, T.; Sellam, F.; Staub, R.; Torker, M.; Fritz, T.; Kübel, C.; Müllen, K.; Leo, K. *Surf. Sci.* **2000**, *445*, 358−367.
(20) Staub, R.; Torker, M.; Fritz, T.; Schmitz-Hübsch, T.; Sellam, F.; Leo, K. *Surf. Sci.* **2000**, *445*, 368−379.
(21) Antohe, S.; Tomozeiu, N.; Gogonea, S. *Phys. Status Solidi A* **1991**, *125*, 397−408.
(22) Uder, B.; Ludwig, C.; Petersen, J.; Gomph, B.; Eisenmenger, W. *Z. Phys. B* **1995**, *97*, 389−390.
(23) Wan, K. J.; Lin, X. F.; Nogami, J. *Phys. Rev. B* **1993**, *47*, 13700−13723.
(24) Upward, M. D.; Beton, P. H.; Moriarty, P. *Surf. Sci.* **1999**, *441*, 21−25.
(25) Sotiriou-Leventis, C.; Mao, Z. *J. Heterocycl. Chem.* **2000**, *37*, 1665−1667.
(26) Chen, Q.; Rada, T.; Bitzer, T.; Richardson, N. V. *Surf. Sci.* **2003**, *547*, 385−393.
(27) Eremtchenko, M.; Schaefer, J. A.; Tautz, F. S. *New J. Phys.* **2003**, *425*, 602−605.